

Investigating the growth graphene as a protective coating on Ir(111) and Fe-22Cr crystals using chemical vapour deposition

Kasper Medium Rasmussen

Studentnumber: 20115156

Thesis submitted to Department of Physics and Astronomy,

Aarhus University

for the Bachelor degree in physics

March 2014

Supervisor: Liv Hornekær

Abstract

Graphene was first isolated in 2004 by A.K. Geim and K.S. Novoselov. Since then a lot of different studies have been carried out to fully understand and utilize graphene.

The aim of this project was to grow graphene on a Fe-22Cr crystal. This is an alloy very similar to the composition of stainless steel. The motivation was that the graphene could be used as a coating to further protect the surface against corrosion. First the surface of the Fe-22Cr crystal had to be investigated fully. During heating of an alloy the surface changes. Therefore it is important to understand how this surface changes.

Before investigating the Fe-22Cr surface, we wanted to practice the growth of graphene on a Ir(111) surface using chemical vapour deposition (CVD) technique. This was done in order to understand the actual growth of graphene. With these initial experiments we gained experience in the use of the CVD technique. The graphene quality was checked by the use of scanning tunnelling microscope (STM) which is able to give atomic resolution images of the surface.

Then the attention moved to the Fe-22Cr crystal. The surface was investigated using STM and Auger electron spectroscopy (AES), the latter is able to show which elements the surface is made of. Using these two techniques we measured the surface before and after heating.

The results show that upon annealing to 600°C there is a migration of chromium towards the surface. This was seen as increments in the intensities in the Auger spectrum and as a change in the STM images. This observation is described in the context of published literature.

Dansk resumé

Grafén blev isoleret for første gang i 2004 af A.K. Geim og K.S. Novoselov. Sidenhen har mange forskellige studier forsøgt at forstå og udnytte grafén.

Hovedmålet med dette project var at gro grafén på en Fe-22Cr krystal. Dette er en legering, meget lignende rustfrit stål. Motivationen var at grafén kunne bruges som en beskyttende belægning for yderligere beskyttelse af overfladen mod korrosion. Først skulle overfladen af Fe-22Cr krystal undersøges fyldtsgørende. Under opvamningen af en legering ændrer overfladen sig. Derfor er det vigtigt at forstå, hvordan netop denne overflade ændrer sig.

Før undersøgelsen af Fe-22Cr krystallen, ville vi først øve os i at gro grafén på en Ir(111) overflade ved at bruge kemisk fordampnings deponering (CVD). Dette blev gjort for at forstå den egentlige groning af grafén. Med disse indledende forsøg opnåede vi erfaring i brugen af CVD teknikken. Kvaliteten af grafénen blev undersøgt ved hjælp af skanning tunnelling microskopi (STM), som er i stand til at lave billeder af overfladen med atomar opløsning.

Derefter rettedes opmærksomheden mod Fe-22Cr krystallen. Overfladen blev undersøgt ved hjælp af STM og Auger elektron spektroskopi (AES), som er i stand til at fortælle, hvilke elementer overfladen består af. Ved at bruge disse to teknikker tog vi målinger af overfladen både før og efter opvarmning.

Resultaterne viser en migration af chrom atomer mod overfladen efter opvarming til 600°C. Dette ses som stigninger i intensiteterne i Auger spektrum og som ndringer på STM billederne. Denne observation er også beskrevet i litteraturen.

Acknowledgements

I would like to thank my supervisor Liv Hornekær for giving me the opportunity do this thesis work in the Surface Dynamics Lab. Secondly a special thanks to everyone working together with me in the lab; Andrew Cassidy, who also has proofread the thesis, Mikkel S. Kongsfelt and Susanne Halkjær. Finally a thanks to the rest of the group in the lab; Jill Miwa, Line Kyhl, Anders Lind Skov and Sune Fuglsang, who also made a nicer version of the diagram of the STM, for their technical support and good company during lab time.

Kasper Medium Rasmussen
Aarhus, March 2014

Contents

Abstract	i
Dansk resumé	ii
Acknowledgements	iii
Acronyms	vi
1 Introduction	1
1.1 Graphene	2
1.2 Growing graphene	3
1.2.1 Mechanical exfoliation	4
1.2.2 Chemical vapour deposition	4
1.3 Graphene as a coating material	5
2 Theory	6
2.1 Graphene	6
2.2 Ultra-high vacuum	6
2.2.1 Mean free path	7
2.2.2 The rate of impinging molecules	7
2.3 Alloys	8
2.4 Scanning tunnelling microscope theory	9
2.5 Auger electron spectroscopy theory	10
3 Experimental	13
3.1 Achieving ultra-high vacuum	13
3.1.1 The chamber	13
3.1.2 Roughing pump	15
3.1.3 Turbo pump	15
3.1.4 Titanium sublimation pump	15

CONTENTS

3.1.5	Ion pump	16
3.1.6	Bake out	16
3.2	Scanning tunnelling microscope operation	17
3.2.1	Scanning tunnelling microscope setup	17
3.2.2	Scanning tunnelling microscope calibration	19
3.2.3	Scanning tunnelling microscope operation modes	20
3.3	Auger electron spectroscopy operation	20
3.4	Cleaning the metal surfaces	20
3.4.1	Ion Gun	21
3.4.2	Anneal	21
3.4.3	O ₂ and H ₂ treatments	21
3.5	Growing graphene on Ir(111)	22
4	Results	23
4.1	Graphene on Ir(111)	23
4.2	Surface of Fe-22Cr crystal	26
5	Conclusion	31
5.1	Outlook	31
Bibliography		33
Appendix A AES manual for the equipment on the Green Chamber A1		

Acronyms

0D zero dimensional.

1D one dimensional.

2D two dimensional.

3D three dimensional.

AES Auger electron spectroscopy.

BCC body-centered cubic.

CVD chemical vapour deposition.

FFT fast Fourier transformation.

HOPG highly ordered pyrolytic graphite.

LDOC local density of states.

SDL Surface Dynamics Lab.

STM scanning tunneling microscope.

TSP titanium sublimation pump.

UHV ultra high vacuum.

1 Introduction

Graphene has been called a wonder material [1]. This is due to its many highly usable properties. Among these are the thickness of only one atom, high conductivity both electronic and thermal and its strength. These, and other properties, make graphene a widely investigated material in the scientific world. Before graphene can be used commercially, however, more research is needed. Research, not only aimed at utilizing these properties, but equally as much in the making of graphene. The methods for making graphene should be both cheap and productive, but must also produce graphene of a high quality. Several methods can be used in the making of graphene, some of these will be discussed later in this thesis.

The motivation for this project is the use of graphene as a coating to protect metals against corrosion. The purpose of this thesis is therefore to investigate the growing of graphene on an alloy, similar to stainless steel, using chemical vapour deposition (CVD). This is done in order to characterize the performance of graphene as a coating, protecting the surface from corrosion. This has been done by firstly preparing graphene on a Ir(111) crystal and later the intention was to grow graphene on a much more complex Fe-22Cr crystal. The results of this thesis focus on the characteristics of the Fe-22Cr crystal upon annealing this crystal. The characterisations has been done with the use of scanning tunnelling microscope (STM) and Auger electron spectroscopy (AES) techniques. Both give data describing the surface of our sample.

The experimental work was done in the period September 2013 to January 2014 in the Surface Dynamics Lab (SDL) at Aarhus University, Aarhus, Denmark, supervised by Liv Hornekær. The first part of the work, where graphene was grown on iridium, was done together with Andrew Cassidy, post doc in the SDL group and Mikkel S. Kongsfelt, Phd. Student from the chemistry department at Aarhus University. The later work on the Fe-22Cr alloy was done together with Susanne Halkjær, master student in the SDL group.

The thesis is divided into five main chapters. Firstly an introduction where graphene and growing methods are described. Secondly, a theory chapter. Here

theory of both materials and experimental equipment used in the project will be described. Thirdly, an experimental chapter. This will in further detail describe some of the experimental equipment and methods used in this project. After this a results chapter, where results are presented. This includes results on both graphene on iridium and the surface investigations of the Fe-22Cr crystal. Finally a conclusions chapter with an outcome section which will describe some suggested further work. This is the first time that the use of AES will be described in a thesis from the SDL group. Therefor, at the very end an appendix will describe the use of the specific Auger spectrometer used in this project. This will be useful later on for other students, who will work with AES in the lab.

1.1 Graphene

Graphene is a monolayer of carbon atoms. This monolayer arranges in a two dimensional (2D) honeycomb lattice. These carbon atoms can then be used as basic building blocks for different carbon materials of other dimensionalities. It can make zero dimensional (0D) fullerenes, one dimensional (1D) nanotubes or three dimensional (3D) graphites by respectively wrapping, rolling or stacking these 2D honeycombs [2].

The discovery of free standing graphene was very surprising and unexpected in the scientific world, because it had for a long time been believed that all 2D crystals were thermodynamically unstable and could therefore not exist [2].

As mentioned in the introduction graphene has some very promising properties. These properties are not only theoretical, but have been observed in laboratories. A room temperature electron mobility of $2.5 \times 10^5 \text{ cm}^2\text{V}^{-1}\text{s}^{-1}$ has been measured[4]. Above 3000 WmK^{-1} has been measured in thermal conductivity. Both of which are better than copper [4]. The strength has also been measured to a Young modulus of 1 TPa [4], in comparison steel has an Young's modulus of 0.2 TPa [5, p. 353]. This means that graphene is rigid and very hard in the x- and y-directions, due to the strong interaction in the carbon bonds. Despite being very strong, graphene is also flexible in the z-direction. Besides these properties, graphene is transparent, but still visible to the naked eye, it has an optical absorbency of 2.3 % [4].

These properties make graphene a prominent component for use in electrical devices, such as touch-screens, e-paper or other flexible electronics. Just as promising is the potential use of graphene in coating or composite materials. Since graphene can be grown on a variety of different metals and combined with its highly inert properties, it could act as a barrier, protecting different metals from oxygen or

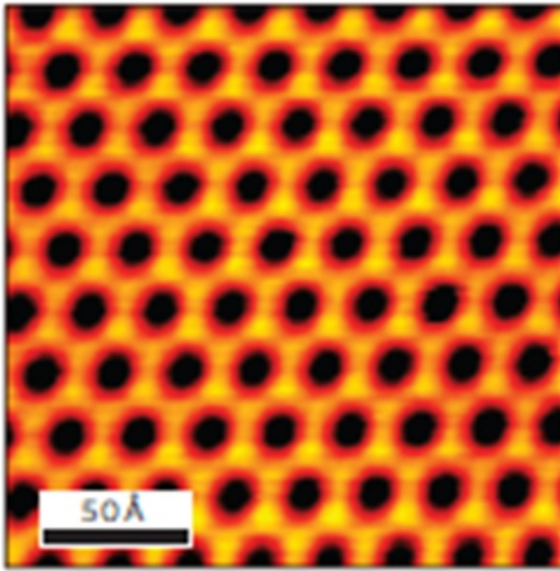


FIGURE 1.1: Graphene on Ir(111) as seen by Scanning Tunneling Microscope. The black dots form a hexagon, which is the Moiré pattern, that graphene on Ir(111) makes [3].

water and thereby preventing corrosion [4]. This is some of the inspiration for the experiments carried out in this thesis. Despite the fact that graphene can be grown on numerous metal surfaces, it is not all of them which is equally easy to work with.

1.2 Growing graphene

There are several ways of preparing graphene or growing it, as it is also called. It is not safe to say that one method is the best. All of these different ways have both advantages and disadvantages. Most of the advantages and disadvantages is related to the cost and the quality of the produced graphene. In this section some of these methods will be discussed in further detail, including the method used in the experiments for this thesis.

When selecting a growth method it is important to keep in mind what the graphene will be used for. Some applications demand good quality with advanced properties, whereas other only demand lower quality graphene, where the numerical value of the properties are lower.

Since the first isolation of graphene in 2004 by A.K. Geim and K.S. Novoselov, there has been a lot of research going into many of these growing methods and some are improving.

1.2.1 Mechanical exfoliation

Mechanical exfoliation, often referred to as the scotch-tape technique, was the method used for the first isolation and studies of graphene [1]. The execution of this method is, as the names indicates, to use scotch-tape to mechanically pull flakes of graphite off a bulk crystal. Geim and Novoselov used highly oriented pyrolytic graphite (HOPG). The peeling is done repeatedly giving few layers thick graphene films of up to 10 μm across, and thicker films up to 100 μm across. These film where then placed on oxidized Si substrates for further analysis [6]. This method produces high quality graphene, but the flakes of the monolayers are rather small, compared to other methods.

1.2.2 Chemical vapour deposition

CVD is a method commonly used in laboratories. The graphene is grown on a metal surface which has been prepared by cleaning it thoroughly. It can be done under arbitrary pressure, ranging from atmospheric pressure to ultra-high vacuum (UHV). When growing in UHV a carbon containing gas is introduced into the chamber, this could be ethylene (C_2H_4). The metal crystal is then heated to a higher temperature. This temperature depends on the metal used. A Cu(111) crystal is heated to about 1000 °C [7].

When the gas molecules hit the hot metal surface, they crack and the hydrogen is lost. The carbon atoms rearrange on the surface, due to the high temperature, thereby forming graphene on the surface. The quality of the grown graphene depends on a lot of different factors; how clean the crystal is before growth, the quality of this crystal, the pressure, the temperature, number of cycles performed etc. All of these parameters should be optimized for the material used.

Due to previous experience in the group, the CVD method was chosen for this project. Using this method the successful growth of graphene has been achieved on several different metal crystals. Therefore we were able to grow graphene of good quality and with good sized domains, here meaning almost the size of our Ir(111) crystal.

Recently a promising development has been achieved in the CVD area. In 2010 S. Bae *et al.* published a paper introducing a roll-on-roll CVD method for growing transparent graphene sheets. These sheets could be produced as large as 30" diagonally. The quality is, however, not the best [8]. This makes the production of graphene on large scale much cheaper and easier. The procedure is briefly explained in figure 1.2.

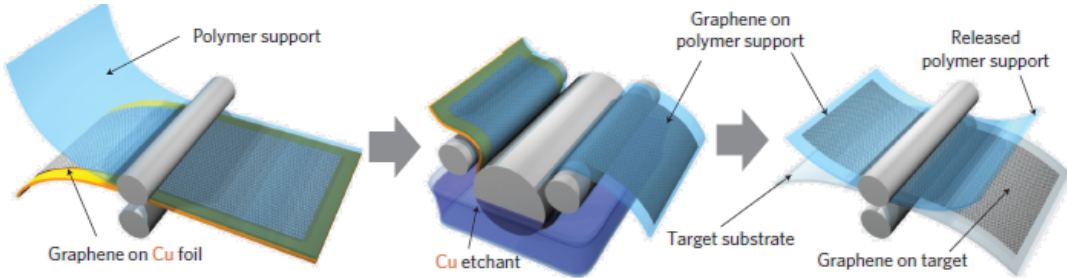


FIGURE 1.2: A schematic view of the production of 30" transparent graphene sheets. The graphene is grown on copper films and a polymer support is bonded on top of it. Then the copper film is etched away, and the graphene is transferred to the target material [8].

1.3 Graphene as a coating material

The ability to protect metals from a reactive environment is highly usable in many different industries and applications. The belief that graphene can be used as a protective coating has resulted in several articles [9, 10, 11, 12]. It is already known that a monolayer of graphene is impermeable to most gasses, including helium [13]. The advantage of using graphene as a protective coating instead of the solutions in use now, is that graphene is very thin and will not change the physical properties of the metal [10].

Nilsson *et al.* showed that a graphene coated Pt(100) surface could be protected from O₂ at a pressure as high as 10⁻⁴ mbar and from CO at pressures below 10⁻⁶ mbar. Chen *et al.* showed that graphene films grown with CVD could be used as a chemically inert barrier to protect both Cu and Cu/Ni alloy from air corrosion even after annealing to 200°C for 4 hours in air. Prasai *et al.* showed that also mechanically transferred graphene could be used to protect Cu and Ni. The metal did corrode at cracks in the graphene, however the graphene itself was not damaged. With CVD grown graphene, Cu could even be protected in an aerated Na₂SO₄ solution.

Besides articles describing the positive effect of graphene as a coating, there is also articles showing a breakdown in the coating effect after cycles of exposure to different gasses [14]. Nilsson *et al.* later reported that a sequential exposure to O₂ and H₂S causes a breakdown in the coating effect. They proposed that the cycles of exposure released the oxygen atom from the platinum surface.

2 Theory

In the results chapter scanning tunnelling microscope (STM) and Auger electron spectroscopy (AES) data will be presented. In order to fully understand these data, the following chapter will describe some of the theory for the equipment and materials used in this project.

2.1 Graphene

When growing graphene on a metallic surface, the graphene adopts a certain pattern depending on which metal it has been grown on. On iridium a superposition of two regular lattices appears. These two regular lattices come from clean iridium and graphene. This new lattice is called the Moiré structure. Its periodicity is much larger than the two original lattices'. The periodicity of the Moiré structure for graphene on Ir(111), the crystal also used in this project, has been measured by Moiré analyses to be (25.3 ± 0.4) Å[15].

It is from these lattices, that is is possible to recognize graphene and even calibrate the experimental equipment. In section 3.2.2 the calibration will be further explained.

2.2 Ultra-high vacuum

All experiments were performed under ultra-high vacuum (UHV). The main reason for this is to keep the surface clean throughout the experiments. In UHV the rest gas has a pressure of 10^{-9} mbar or less. In the chamber used in this project, we preferably work at a pressure in the order of 10^{-10} mbar. When working with vacuum there are two quantities which can be very illustrative to calculate; The mean free path and the rate at which molecules hit the surface [16].

2.2.1 Mean free path

The mean free path is defined as the mean distance travelled by a molecule between collisions with other molecules. This distance, λ , is given by

$$\lambda = \frac{k_B T}{\sqrt{2\pi}\xi^2 P} \quad (2.1)$$

Here k_B is the Boltzmann constant in J/K, T is the temperature of the gas in K, ξ is the molecular diameter in m and P is the pressure in Pa. It is clearly seen, that this distance will be much greater for UHV than for normal atmospheric pressure.

If one were to do the calculation for e.g. nitrogen, the result for atmospheric pressure would be in the order of nm, while for UHV it would be in the order of km. This highly increases the chance of the molecules hitting the wall instead of hitting other molecules [16].

2.2.2 The rate of impinging molecules

As mentioned earlier, the main reason for using UHV is to keep the crystal clean. The crystal gets dirty when molecules hit and stick to it. Therefore, it is in our interest to calculate at what rate molecules are hitting the surface of the crystal. This rate, R , is given by

$$R = \frac{P}{\sqrt{2\pi M k_B T}} = \frac{2.635 \times 10^{22} P_{\text{mbar}}}{\sqrt{MT}} \text{ cm}^{-2} \text{s}^{-1} \quad (2.2)$$

Here M is the molecular mass in units of the atomic mass constant. We see that the rate is proportional with the pressure, and therefore the rate will decrease when the pressure gets smaller [16].

Doing a quick estimate of this rate for different molecules, we can use a pressure of 10^{-9} mbar and a temperature of 300 K, which is about room temperature.

H_2 , where $M = 2$, gives $R = 1.1^{12} \text{ cm}^{-2} \text{s}^{-1}$.

N_2 , where $M = 28$, gives $R = 2.9^{11} \text{ cm}^{-2} \text{s}^{-1}$.

O_2 , where $M = 16$, gives $R = 3.8^{11} \text{ cm}^{-2} \text{s}^{-1}$.

A surface has, in the order of magnitude, about 10^{15} atoms per cm^2 . The molecules described above is only some of the molecules in the rest gas. It does show that if all of the above molecules sticks to the surface, the surface will stay clean for around 100 seconds, i.e. after this time every surface atom will now have a molecule stuck onto it. This shows that the surface stay cleaner much longer in UHV, thereby enabling the experiment to run for longer time without interference

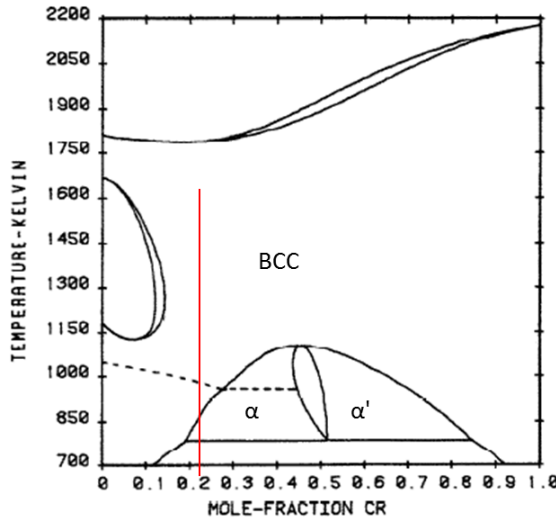


FIGURE 2.1: Complete phase diagram of the Fe-Cr system. The BCC phase under the dashed line is ferromagnetic [18]. α indicates a iron rich phase and α' is an chromium rich phase. The red line indicates the composition of the crystal used in this project.

from a dirty surface [16].

2.3 Alloys

When considering a system of only one component all phases have the same composition and the only variables are the temperature and the pressure. When considering alloys the composition is also a variable which needs to be taken into account. To simplify this we assume that every transformation occurs at a non-variable pressure, which is reasonable since we only operate in the solid phase of the alloy, therefore we only have to take into account the temperature and composition of the alloy [17]. In this project an alloy consisting of iron (Fe) and chromium (Cr) has been examined. These elements are completely soluble in their liquid phase. In their solid phase, however, they show a miscibility gap in which both an iron rich and a chromium rich phase exist. This can be seen on the phase diagram in figure 2.1. In this figure the composition of our crystal is also showed.

What happens when alloys consisting of Fe-Cr are heated has been an motivating factor for several articles [19, 20, 21]. Ali-Löytty *et al.* showed that the CrN concentration on the surface of their Fe-17Cr crystal increased after heating it to 527°C. N is the main contaminant in the bulk crystal. Lin *et al.* got a similar result. They heated their Fe-20Cr crystal to 833 K for 30 min. and observed the formation of a clean CrN overlayer. They then performed AES and according to the

Auger spectrum the overlayer was without impurities and the concentration of Cr was calculated to be twice of that of the concentration of Cr in the bulk, indicating a Cr enrichment on the surface. This points to the fact that Cr diffuses from the bulk to the surface. It is believed that it is this CrN layer that gives a passive layer which protects the alloys from corrosion, hence making it stainless.

2.4 Scanning tunnelling microscope theory

With STM it is possible to, indirectly, get a topographic picture of a surface. The STM gives a map of the local density of states (LDOS). When scanning on metal surfaces this LDOS maps can be deciphered as the topography of the surface.

It is a quantum phenomena that makes it possible to use STM. When a voltage is applied between the tip of the STM and the sample surface, and both of these are conducting, there is a probability for electrons to tunnel from one to the other. When the distance between these two is made smaller this probability gets bigger. This will happen both in air and in vacuum, making it possible to examine surfaces under different circumstances. Due to the tunnelling current being highly depending on the distance between the tip and the surface, precise recordings of the structures of the surface are possible.

In order to explain the theory behind STM Tersoff and Hamann [22, 23] introduced some simplifications and approximations. One important simplification was suggested by Bardeen [24]. It was assumed that the wave functions for the tip and the sample could be treated separately or as unperturbed wave functions [25]. The tunnelling current can be given to the first order in the formalism from Bardeen [24]. When taking into account that most studies are done at room temperature or below and at small voltage, approx 10 meV, the current can be given as

$$I = \frac{2\pi}{\hbar} e^2 V \sum_{\mu\nu} |M_{\mu\nu}|^2 \delta(E_v - E_F) \delta(E_\mu - E_F) \quad (2.3)$$

Here V is the applied voltage, $M_{\mu\nu}$ is the tunnelling matrix element between the states ψ_μ of the tip and ψ_v of the surface and E_μ is the energy of state ψ_μ in the absence of tunnelling.

In the special case where the tip is a point probe, equation 2.3 reduces to

$$I \propto \sum_v |\psi_v(\vec{r}_0)|^2 \delta(E_v - E_F) \quad (2.4)$$

Then the matrix element simply becomes proportional to the amplitude of ψ_v at the

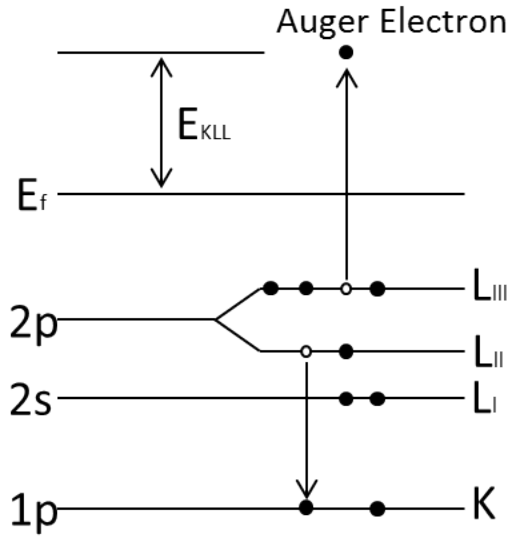


FIGURE 2.2: Schematic diagram of the Auger electron emission. Figure is made as a replicate from [26].

position of the probe \vec{r}_0 . In equation 2.4 the right side is the surface LDOS at the Fermi energy, E_F .

A current tunnelling through a barrier, e.g. vacuum, is proportional to $e^{-2\kappa d}$ giving the following

$$I \propto \rho(\vec{r}_0, E_F) e^{-2\kappa d} \quad (2.5)$$

Where $\rho(\vec{r}_0, E_F)$ is LDOS at the Fermi energy at the point \vec{r}_0 , $\kappa = \hbar/(2m\phi)^{1/2}$ where m is the mass and ϕ is the local workfuntion [25].

Here the most important feature of STM is shown. STM displays the LDOS at the Fermi energy. This represents the positions of the atoms, but in reality it images the electron density related to the individual atoms. The reason that STM is so precise and capable of displaying atomic resolution is the exponential factor. This gives a significant change in the tunnelling current when the distance between the tip and surface changes by only a few Å.

2.5 Auger electron spectroscopy theory

With AES it is possible to get a spectra showing which elements the top most layers of a sample are made of.

A sample surface is irradiated with a beam of electrons. Due to collisions between an incident electron and one from the inner shell of a surface atom, a hole in the inner shell is created. This causes the atom to be excited into an excited state, which

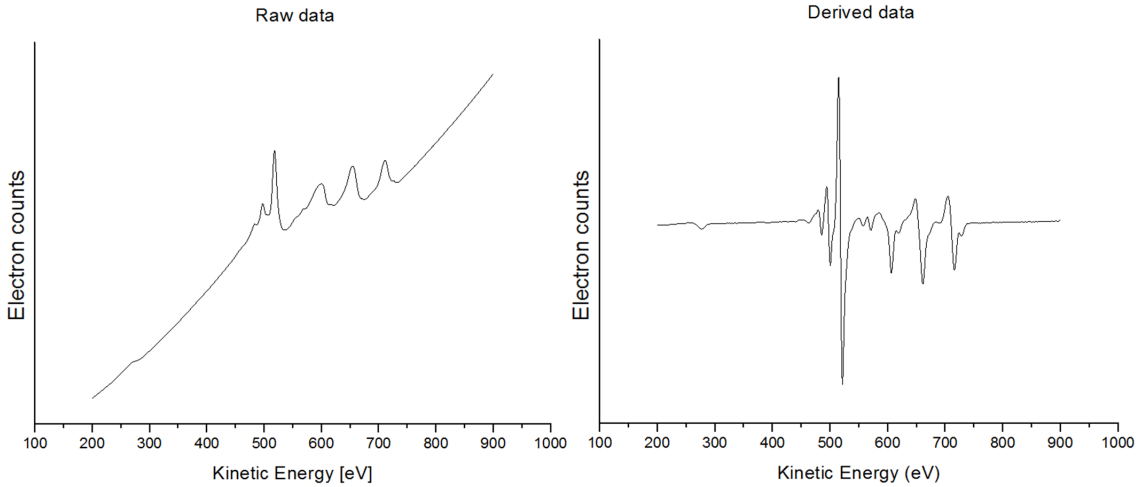


FIGURE 2.3: An example of an AES measurement on the Fe-22Cr crystal. The raw data has been derived in order to create a peak structure where the elements are easier to identify. This is due to the domination of the backscattered electrons in the raw data.

is also an unstable state. To return the atom to a low energy state, an electron from an outer shell falls down to fill the recently created hole. The process is illustrated in figure 2.2. The energy difference between these two orbital shells can now be transferred to another outer shell electron. If the transferred energy is greater than the binding energy of this receiving electron, the electron is emitted from the surface. This emitted electron is referred to as an Auger electron [26]. The reason that only the top layers can be analysed is that the Auger electron must escape the surface. This is impossible if the Auger electron is emitted from the bulk, due to collisions with other atoms.

An example of an Auger spectrum is seen in figure 2.3, displayed as both raw data and the derivative of this data. The Auger spectrum is a plot of the number of electrons emitted from the surface versus the kinetic energy of these electrons. Due to the domination of back scattered electrons in the spectra, the spectra is typically represented as the derivative of the raw data, thus creating a peak structure, and the elements can be identified by the position of these peaks. The principle behind AES is the same as the one used in X-ray fluorescence. The difference is that in X-ray, photons with a X-ray energy are emitted and here it is electrons with an Auger energy. This makes AES more usable for surface measurements, since an Auger electron will have a great difficulty escaping the bulk of a sample due to the possibility of hitting numerous atoms in the sample.

Auger transitions are labelled by the energies of the involved electrons. In figure 2.2 it is an KLL transition. K is the initial core hole, L_{II} and L_{III} are the

THEORY

initial energy levels of the electrons involved in the Auger transition. This can be abbreviated to *KLL*[26].

The energy of the emitted Auger electron can also be found theoretically. It is equal to the energy difference between the double ionized final state and the single ionized first state. This can be estimated as the difference in the energy levels of the atom. Using general notation, such as an arbitrary Auger transition of an atom with atomic number z , the energy of an *ABC* transition is as follows,

$$E_{ABC}(z) = E_A(z) - E_B(z) - E_C^*(z) - \phi_s \quad (2.6)$$

where E_A , E_B and E_C^* are the binding energies of the corresponding energy levels A B and C. ϕ_s is the work function of the spectrometer, which can be neglected in a theoretical analysis, since it is only required if we want to measure the energy of the Auger electron. The second to last term of equation 2.6 can then be approximated to the binding energy of a slightly more massive neutral atom with atomic number $z + \Delta$, when $0.5 > \Delta > 1.5$ [26],

$$E_{ABC}(z) = E_A(z) - E_B(z) - E_C(z + \Delta) \quad (2.7)$$

A different empirical approximation, was suggested by Chung and Jenkins [27]

$$E_{ABC}(z) = E_A(z) - \frac{1}{2}[E_B(z) + E_B(z + 1)] - \frac{1}{2}[E_C(z) + E_C(z + 1)] \quad (2.8)$$

The calculation of the Auger energies was published in tables and the Auger peaks could be identified using such tables. Now, however, it is easier to use a reference spectrum from a compilation of experimentally acquired spectra [26].

3 Experimental

In the following section some of the equipment used in this project will be described in detail. First there will be given a description of the method for achieving ultra-high vacuum (UHV). Following this, there will be a description of the main techniques used for the experimental work in this project, scanning tunnelling microscope (STM) and Auger electron spectroscopy (AES).

3.1 Achieving ultra-high vacuum

A consequence of UHV is that the rest gas will not flow like gas at ambient pressure. At UHV the flow is called molecular, while it is called viscous flow at ambient pressure. This different behaviour requires different pumps to work in series, each of these should have their own characteristics, in order to achieve and maintain UHV. A schematic view of this setup, with the chamber and different pumps, can be seen in figure 3.3. Some of these will be described in the following section. The first thing needed to achieve UHV is a leak-tight chamber, this will also be described.

3.1.1 The chamber

The chamber used in this project is called the Green Chamber. Is it located at the Physics and Astronomy Department of Aarhus University, at the Surface Dynamics Lab (SDL). Is it a steel chamber equipped with several components for working and measuring in UHV. Wherever there is a connection, it has to be sealed with a flange. A copper gasket is placed between these flanges. The flanges have knife edges that cut into these gaskets, thereby making an effective leak tight seal. A picture of the chamber and some of the equipment can be seen in figure 3.1.

A manipulator on the top of the chamber allows us to control the direction of the sample in all three spacial directions and rotation, ensuring that we can point it towards all equipment attached to the chamber. The filament used for heating the crystal is place behind the sample holder on the manipulator. Due to the technical

EXPERIMENTAL

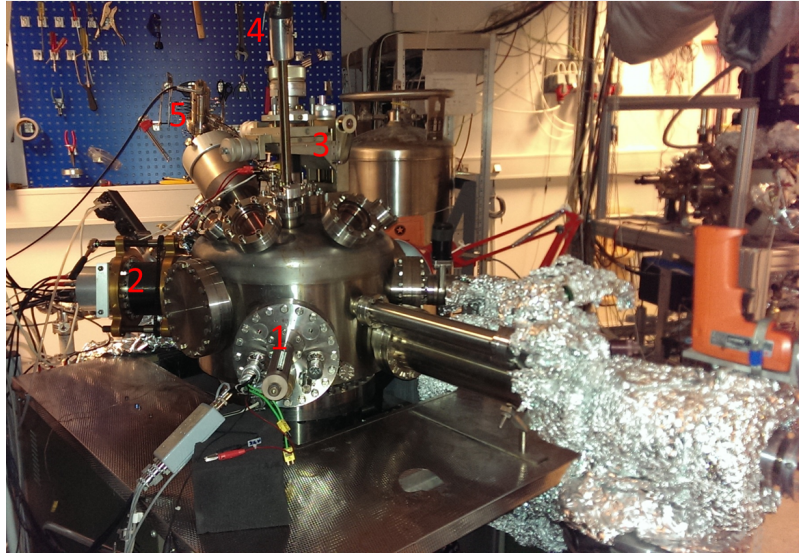


FIGURE 3.1: The Green Chamber. 1: STM, 2: AES, 3: Manipulator, 4: Wobble-stick, 5: Iongun. Not seen on the picture is the mass spectrometer, placed at the back of the chamber.

difficulties in heating a sample to high enough temperatures, the filament was often the reason for some delays. It often melted or shorted to ground, meaning that it would break. This meant opening the chamber in order to change the filament.

A wobble stick enables us to move the sample around inside the chamber without having to open it. The chamber is also equipped with a load lock so samples can be taken in and out of the chamber again without opening it. It is very important to take care when using the wobble stick. It is during transfer that the sample has the highest risk of being dropped to the bottom of the chamber. If this happens the chamber has to be opened, causing delays and possible damage to the sample.

For cleaning the sample there is an ion gun. This accelerates argon ions towards the surface. These ions hit off impurities from the surface of the sample. This makes the surface atomic rough and therefore heating is needed a rearrange the surface. The cleaning is described in detail in section 3.4.

For measurements in this project primarily the STM and AES techniques were used. These are explained in further detail in sections 3.2 and 3.3. Furthermore, the chamber also has a mass spectrometer attached, which has not been used for experiments in this project. It was, however, used for leak testing the chamber after it had been opened. Leak testing involves using the mass spectrometer to scan for helium. Then a gas bottle with helium which has a needle or small nozzle attached is used to introduce the helium at the flange which has been changed after the opening of the chamber. When the mass spectrometer does not show any increase

in the detected helium, the chamber is deemed leak tight. If not the bolts around the flange should be tightened. During the work on this project several valves were found to be leaking, causing delays, especially towards the end of laboratory time.

3.1.2 Roughing pump

When trying to achieve UHV, the first stage of pumping is done by the use of a roughing pump. This is a powerful pump used to bring the pressure down in the 10^{-3} mbar area. This is also called the backing pressure. Here the gas still has a somewhat normal gas flow. These pumps do not work in conditions lower than this pressure. The roughing pump used on the Green Chamber is an oil-sealed rotary vane pump. It works in two stages. First it seals the outlet and opens to the chamber, thereby expanding the volume of the chamber, allowing gas to enter the pump. Secondly it seals off to the chamber and pushes out the trapped gas. This two-stage function is also why it cannot work in UHV. The mean free path, see section 2.2.1, is simply too high for the gas to flow into the pump [28, 29].

The thing to be careful with, when working with oil-sealed pumps, is backstream. When the pump is switched off oil can run back into the vacuum system. It can however be prevented by using a valve to seal off the chamber before switching off the pump [29].

3.1.3 Turbo pump

To get the pressure even lower than the backing pressure a turbo pump is often chosen. It is made up of a series of rotor blades, spinning at a speed of up to 80.000 rpm. It works by adding momentum to the gas molecules. The momentum of the gas molecules now ensures that the gas is removed from the system.

Unfortunately, this pump does not work effectively for light gas molecules such as hydrogen. For these molecules an additional pump is needed [30]. To minimize the load on the turbo pump, it is important not to have it operating at too high pressure. Therefore it is crucial that the backing pressure is low enough to ensure a well working pumping system.

3.1.4 Titanium sublimation pump

The titanium sublimation pump (TSP) is a more effective type of pump for removal of hydrogen from the chamber. It works via the high voltage heating of a titanium wire to sublimation point. Reactive titanium is then released in the chamber. This

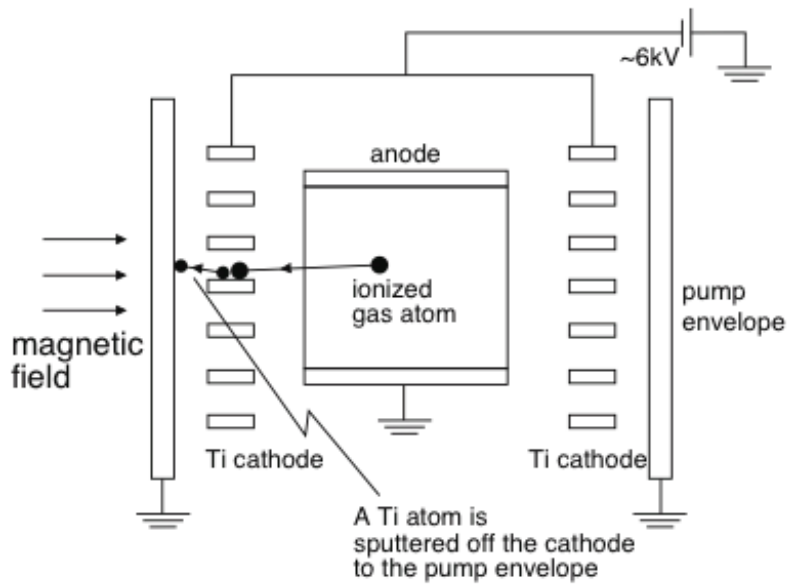


FIGURE 3.2: Schematic view of an ion pump. It is used to maintain the pressure in the UHV chamber [31].

traps some of the rest gas in the chamber. Due to the roughing and turbo pumps' ineffectiveness with pumping out hydrogen, a significant part of this rest gas will consist of hydrogen.

The effect of this pump can be increased by cooling it with liquid nitrogen, thereby making it also work as a cold trap. This then traps ions and molecules more efficiently due to physisorption.

3.1.5 Ion pump

When UHV has been achieved by the roughing and turbo pumping system, the pressure can be maintained by the use of an ion pump. A schematic view of this pump can be seen in figure 3.2. It works by ionizing the rest gas with a high voltage. The ionized gas then hits a titanium cathode and gets buried into it. Like the TSP it does not remove the gas from the chamber, but traps it, thereby preventing it from contributing to the pressure [31].

3.1.6 Bake out

Even with all of these pumping system, UHV is not easily achieved. This is due to the chamber walls having absorbed gas and water vapour. To speed up the removal of these absorbates the chamber can be baked. The Green chamber was heated to 140°C for about 18 hours to ensure that everything on the chamber was heated and

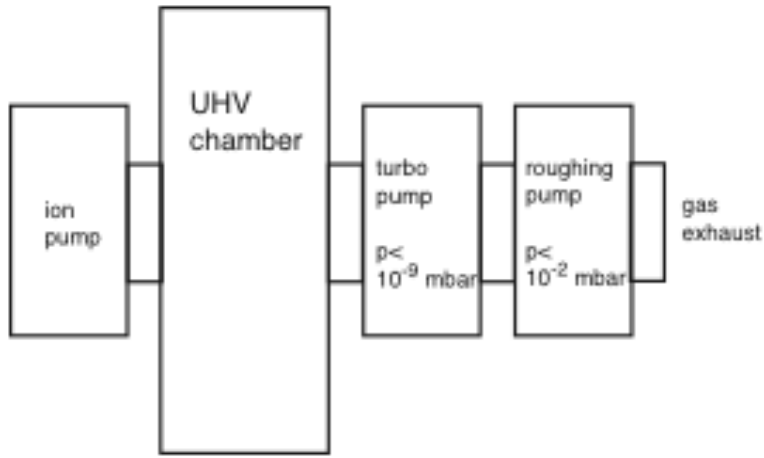


FIGURE 3.3: Schematic view of a UHV chamber and the pumps attach to it. It is important to note how the pumps are very close to the chamber, due to the long mean free path of particles in UHV [32].

all of the water was removed.

This is also why there is a lot of aluminium foil on the chamber on figure 3.1. It is used during the heating, ensuring that everything is heated evenly. This prevents the windows and ceramics from cracking [33].

When the chamber is cooling down, it is important to degas all the filaments. This is done by turning on the filaments and equipment containing filaments when the temperature is higher than it is under normal operation. This ensures that a big desorption of the absorbed rest gas is prevented when the filaments are used later on.

3.2 Scanning tunnelling microscope operation

The first STM was developed by G. Binning and H. Rohrer in 1982 at IBM Zurich Research Laboratory in Switzerland [34]. By using STM in this project we were able to determine the quality of the graphene. In the following section the setup and experimental operation of the STM will be described.

3.2.1 Scanning tunnelling microscope setup

The STM used in the SDL group is designed and developed in Aarhus and is called an *Aarhus STM*. It was designed to give atomic resolution in air. The fact that the STM was developed in Aarhus gives the advantage of having in-house experts to do quick repairs and provide further technical assistance. The *Aarhus STM* is

EXPERIMENTAL

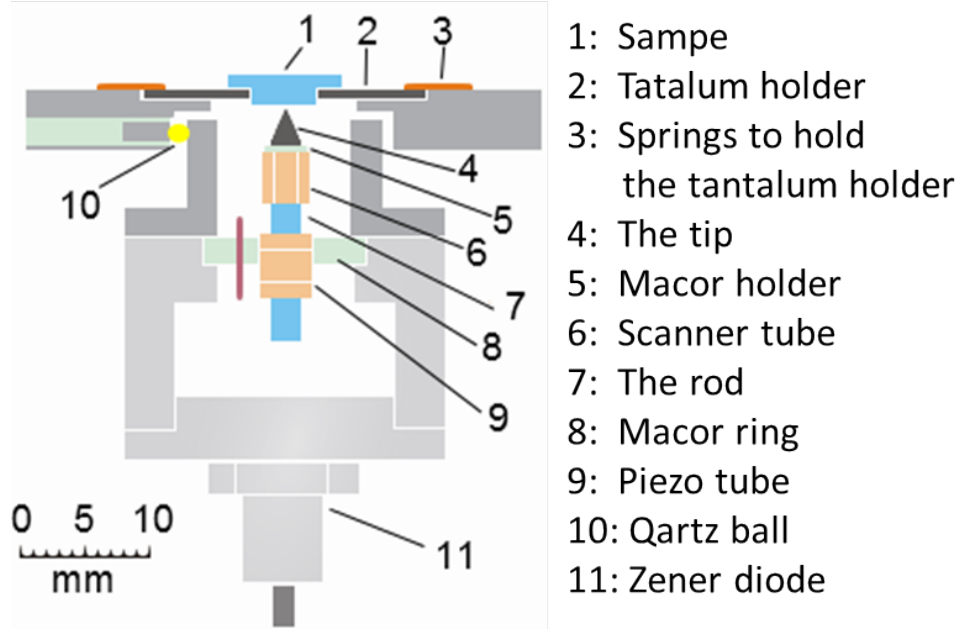


FIGURE 3.4: Schematic view of the Aarhus STM. The image is made as a replicate from [36]. A more detailed explanation is in section 3.2.1.

now a licensed product available from *SPECS Surface Nano Analysis*, a German manufacturer of systems for surface analysis [35]. A schematic view of the STM can be seen in figure 3.4.

The sample is placed in a tantalum holder. Tantalum is used due to its thermal properties. Even when heated to very high temperatures, around 1250°C, it does not deform. Furthermore it is also relatively non-reactive. This tantalum holder is held on to the top plate of the STM by springs.

The tip is made from a conductive material allowing electrons to tunnel through the gap between it and the sample. The images come out best, i.e. minimal noise interference, if the tip is made up of only one atom. This can be achieved by doing tip treatment. There is a lot of different ways of doing tip treatment, one way is to ramp up the voltage between the tip and the sample. This can be done under vacuum, minimizing the disruptions that might occur from tip replacements.

The tip is held by a holder made of macor. Macor is a machinable glass ceramic made by Corning Inc., a world wide manufacture of ceramics for different purposes. Macor is highly machinable allowing complicated shape designs. Furthermore the material does not outgas in UHV, ensuring that it does not contaminate the chamber. Finally it is thermally stable at an operating temperature of 800°C and at a maximum temperature of 1000°C [37].

The scanner tube is made from piezoelectric material. By using the reversed

piezoelectric effect the tip can be moved very accurately in the x- and y-directions. The reversed piezoelectric effect is an effect that can occur in certain solids. When applying a voltage a mechanical strain within the material will cause it to deform.

The rod and the piezo tube serve as a small inchworm motor used for the coarse approaching of the sample. The piezo tube is formed by three rings. When applying a voltage to the center ring it will elongate or contract. The two other rings will clamp on to the rod when a positive voltage is applying and release it when a negative is applied. Because the piezo tube is fixed on to the body of the STM by the macor ring, a correct sequence will move the rod towards or away from the sample. This motor will work in steps down to 2 Å and a maximum speed of 2 mm/min [36].

The aluminium block, which the STM top plate is mounted on, can be cooled with liquid nitrogen. To ensure that the STM does not get too cold the body of the STM is thermally insulated from the top plate with three quartz balls, these also electrically insulate the STM. Furthermore a Zener diode is use to counter heat the STM body when cooling is applied [36].

3.2.2 Scanning tunnelling microscope calibration

A calibration of the STM is needed because the STM uses, as explained in section 3.2.1, piezoelectric elements. The performance of these piezoelectric elements are highly dependent of the temperature, the age and wear. In the experiments in this project the STM was, however, not cooled with liquid nitrogen, meaning that the temperature of the STM was the same as the room temperature in the lab and also relatively constant. This makes the errors from the temperature dependence smaller, a calibration though, is still needed.

It is done be measuring some known pattern on the image and comparing this with a theoretical value. This could be the previously mentioned Moiré pattern from graphene on iridium, see section 2.1. This was done when checking the quality of the chemical vapour deposition (CVD) grown graphene on iridium.

When looking at the surface of the Fe-Cr crystal, there are no such known patterns or structures. Here the best way to calibrate the STM is to scan on another crystal. Preferably one that is easy to scan on. For this we have used highly oriented pyrolytic graphite (HOPG). before scanning on HOPG no cleaning is needed, it only needs to be annealed. Is also has the advantage that it can be used to make a more stable tip, since it can handle rough tip treatments. There is, unfortunately, a possibility to pick up a carbon atom, hence making a bad tip. The surface of the HOPG will , however, not change much during tip treatments. The reason for

wanting a good tip is that a better and more stable tip will reduce noise on the images.

3.2.3 Scanning tunnelling microscope operation modes

There are two different modes in which the the STM can be run; *Constant Height* and *Constant Current*. Both have advantages and disadvantages. In *Constant Height* mode the tip approaches the surface and then stays at this designated hight. When scanning over the surface the change in the tunnelling current is recorded as data. Here there is no feedback making this the faster scanning mode, however it is also the one with less tip stability and there is a risk of crashing the tip into defects or dirt (molecules) on the surface. The *Constant Current* mode uses a feedback loop to keep the tunnelling current constant by changing the z-positioning of the tip. This is then recorded as data. This is slower but provides better tip stability and a lower risk of damaging the tip. This was the method used for this project since the advantage of better image quality rose above the time disadvantage, because the samples were relatively stable and did not change therefore more time could be spent scanning.

3.3 Auger electron spectroscopy operation

AES was used in this project to detect chemical changes in the top layers of crystals. It is important, however, to accept that here the AES gives qualitative descriptions rather than quantitative of how the stoichiometry changes, meaning it cannot show how much it has changed, only what has changed. It will however show if there is more or less of a certain element.

The Auger spectrometer used on the Green Chamber is rather old and has not been operated for several years. Therefore a lot of time was spent resolving the instrumental problems. The hardest problem was getting the control box and the computer to communicate properly. Since this is the first thesis from the group explaining AES, I have made a detailed recipe for operating this specific Auger spectrometer, which is found in appendix A.

3.4 Cleaning the metal surfaces

When UHV is achieved, the surface of the crystal needs to be cleaned before experiments can begin. The cleaning process differs, depending on the material to be

cleaned. In the following section some cleaning methods will be discussed.

3.4.1 Ion Gun

For cleaning metal surfaces ion bombardment or sputtering is very effective. The principle in sputtering is that a noble gas, we use argon, is ionized and accelerated towards the sample. This will then hit off impurities on the surface. It is done, in the Green chamber, at an energy of 2 KeV. After sputtering the surface it is not atomically smooth any more. It has been heavily damaged and the need for annealing, see below, is great. This sputter treatment can, however, change the stoichiometry in compounds, since some elements are easier removed than others [38].

3.4.2 Anneal

After the sputtering the crystal must be annealed to rearrange the surface. Annealing smooths out the surface and removes the bumps and holes created by the argon ions. It is usually done with a even temperature ramp, 1 K/s, to some specific maximum temperature, were the sample is held for a certain time. The target temperature and holding time depends on which metal is used and how clean it is. If the sample is very dirty, e.g. after being used for experiments at another lab, it is important not to heat the sample to too high temperatures, since all the impurities will then come off at once, which will make the chamber dirty and not able to stay in the UHV pressure range. After the holding time an even down ramp is used to allow the crystals to cool, -1 K/s.

Sometimes heating will also draw absorbed molecules dissolved in the bulk to the surface, see section 2.3, were it can be sputtered off. Therefore several cycles of sputtering and annealing are needed [38].

3.4.3 O₂ and H₂ treatments

After successful sputter and anneal cycles, oxygen and hydrogen can be used to remove unwanted impurities. This is done by back-filling the chamber with oxygen to a certain pressure and then the temperature of the sample is ramped up and down between two predetermined temperatures. This is done a certain number of times to ensure maximum effect. This will remove carbon atoms from the crystal. The pressure is then pumped back down to UHV and the next treatment can begin.

After cleaning with oxygen, hydrogen is often used. This will remove leftover

oxygen by creating desorbing water [38]. The procedure is the same as before; the pressure is raised, this time with hydrogen, and then the temperature is raised between two temperatures, also several times. These treatments can be altered to optimize their effect.

During this project the following pressures and temperatures was used. Oxygen treatment; 4.5×10^{-8} mbar, temperature from 400°C to 800°C. Hydrogen treatment; 8×10^{-7} mbar, temperature from 300°C to 800°C.

3.5 Growing graphene on Ir(111)

In this project graphene was grown on an iridium crystal. This was done as a practice of the growth of graphene using CVD. Iridium was chosen because there is a strong interaction between it and graphene, helping to ensure the grown graphene is of a high quality and of the same orientation. The interaction is, however, not so strong that it is impossible to transfer the graphene from the surface of the iridium. Furthermore iridium was also chosen as the group already had experience with this metal and the knowledge of how to grow graphene on this surface. The real desire of this project was to grow graphene on a Fe-22Cr crystal, but the growing on iridium provided a good practice.

Our recipe for cleaning and growing graphene is not new, but is continually modified and improved. The best recipe used in this thesis consists of a series of cycles with both oxygen and hydrogen treatments, immediately followed by cycles of heating and cooling the crystal in an ethylene rich atmosphere.

First the crystal was cleaned with sputter and annealing. This was done with a sputter pressure of 4.4×10^{-7} mbar for 10 minutes, then annealing to 900°C with a 10 minute holding at maximum temperature. After this cleaning the crystal was examined by STM to check if it was clean enough. If the crystal was clean the growing continued, otherwise the crystal would go through a new round of sputter and anneal cycles. The clean crystal then went on for chemical cleaning. Four oxygen treatments followed by two hydrogen treatments were carried out. Promptly after these treatments the actual growing started. The crystal was introduced to a pressure of 4×10^{-7} mbar of ethylene, while the temperature was flashed to 1200°C. Then the temperature was reduced to 900°C and the pressure was increased to 6×10^{-6} mbar. At this pressure, the temperature was raised to 900°C and kept for one minute, then the temperature was raised to 1200°C and kept for a minute. After this the temperature was slowly ramped down to 900°C at which point the ethylene was closed off. The sample was then very slowly cooled to room temperature.

4 Results

The motivation for this project was to investigate the potential use of graphene as a protective coating. In order to do this, we first wanted to grow graphene on another metal crystal as practice for the growth on the Fe-22Cr crystal. Secondly the surface of an alloy will change when it is heated, therefore we wanted to investigate how this surface changes. In the following chapter the results of this project will be presented and discussed. It consists of two sections, one for graphene on iridium and another for the surface analysis of the Fe-22Cr crystal.

4.1 Graphene on Ir(111)

When analysing the scanning tunnelling microscope (STM) images a calibration of the STM is needed. This can be done with a program which also can do fast Fourier transformation (FFT) analysis on the images, and thereby remove noise from the raw images.

Figure 4.1 shows a complete coverage of graphene on a rather large area on the iridium crystal. This graphene is of good quality with few impurities or defects. There is a step edge across the image, but when looking closely it can be seen that the orientation is the same across the step edge, indicating high quality graphene. The spots on the image are probably impurities on top of the graphene or defects which may have been created by impurities that were not cleaned off the crystal before the growing of the graphene. This image represents one of several examples of graphene grown on iridium. The growth was done several times all resulting in graphene with a quality very similar to this. This image was also the image used for the calibration of the STM. The calibration parameters were found to be

$$X : 1.101, Y : 1.077 \quad (4.1)$$

After the calibration there still appears to be an off-set. This is due to drift in the STM.

RESULTS

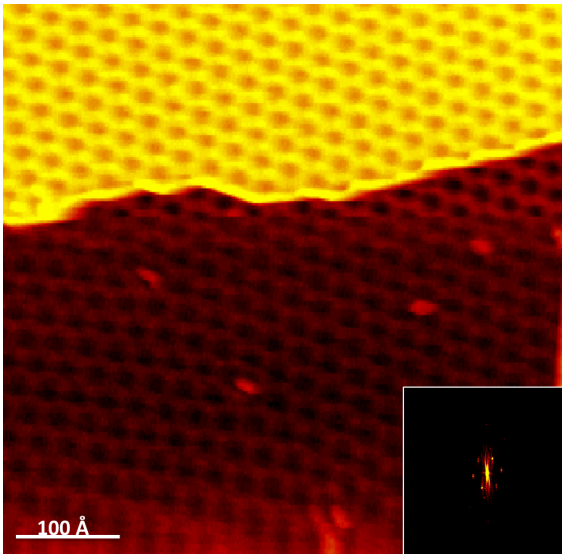


FIGURE 4.1: A STM image of graphene on Ir(111) Grown with the method described in section 3.5. The graphene is of good quality with minor defect or impurities. This is also the image which was used for the calibration of the STM for the graphene on iridium part of the project. $I = -0.640 \text{ nA}$, $V = -103.5 \text{ mV}$.

The samples of graphene grown on iridium in this project were passed on to a group of chemists at the Chemistry Department at Aarhus University. They wanted to transfer the graphene from the iridium to SiO_2 wafers. This is because iridium is a conductor and in order to get full use of graphene in electrical devices, it should be transferred to a semiconductor or as in this case an insulator. They do this transfer using electro chemistry to intercalate hydrogen between the graphene and the iridium surface. Their intention is to patent the exact method. After, what was believed to be, a successful transfer the crystal was returned to our laboratory to do further STM to check if the graphene had been removed.

In figure 4.2 a STM image of the iridium surface after the transfer is shown. No graphene, i.e. Moiré structures, are visible, meaning that the transfer was in fact successful. Additionally a step edge can also be seen on the left side of the image. Furthermore the surface does not look very dirty, meaning that there are no islands of graphene left from the transfer. On figure 4.3 two optical pictures of the iridium crystal after transfer can be seen. The fact that the graphene has been transferred is even visible for the eye. There is a clear difference from the center to the outer part of the crystal, again indicating a successful transfer. Later analysis done by the chemists also showed a successful transfer.

Our success with growth of graphene on iridium continued until we moved on with the project. Now the attention was aimed at the Fe-22Cr crystal.

RESULTS

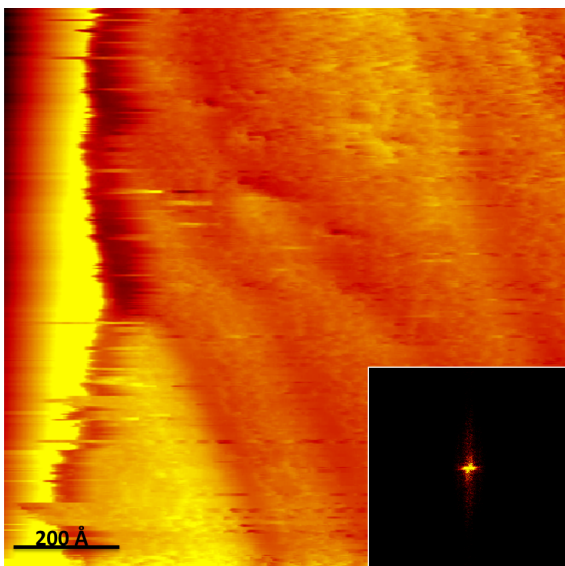


FIGURE 4.2: A STM image of the iridium sample after the chemist had tried to transfer the graphene. It looks successful, since no graphene is now visible. $I = -3.910 \text{ nA}$, $V = -84.5 \text{ mV}$.

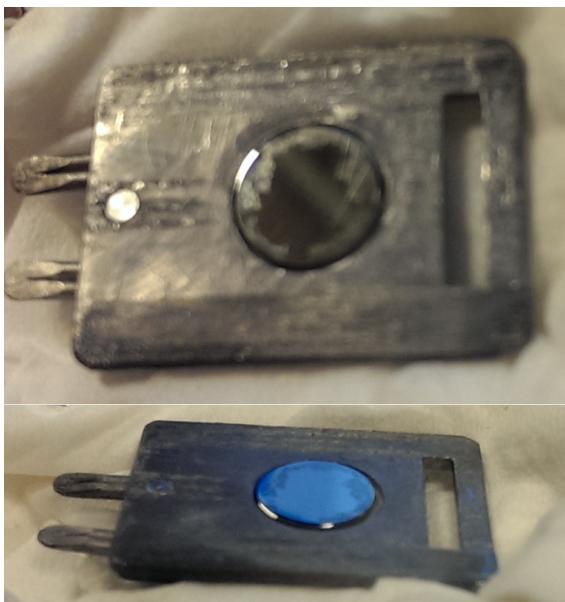


FIGURE 4.3: Two pictures of the same Ir(111) crystal, from different angles, after the graphene has been transferred off by the chemists. There is a clear difference from the middle to the edge of the round crystal, indicating that something has been removed from the surface.

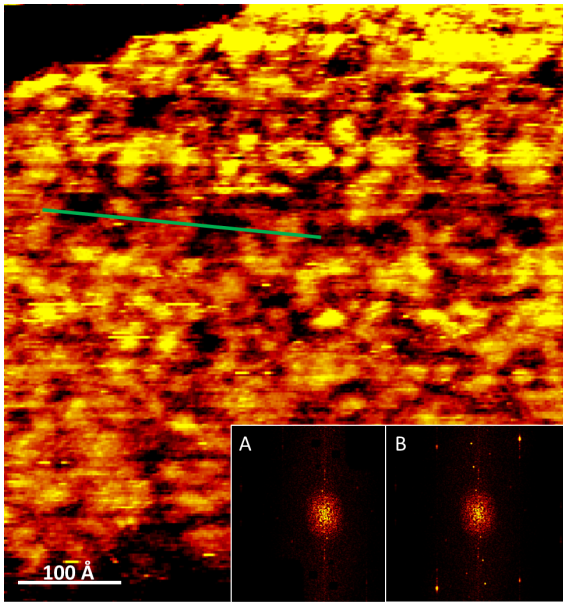


FIGURE 4.4: A STM image of the clean Fe-22Cr surface. The image has been filtered with the use of a FFT program, which can remove noise. The inserts displays the FFT before (B) and after (A) filtering. The green line represents the line scan in figure 4.6A. $I = 0.430 \text{ nA}$, $V = 1250 \text{ mV}$.

4.2 Surface of Fe-22Cr crystal

The crystal is an alloy consisting of iron with 22% chromium. As mentioned in the theory, section 2.3, the surface of an alloy can change when heated. Articles in the literature point to a new surface where chromium has migrated from the bulk to the surface. Therefore, it is important to investigate what happens when our crystal is heated, i.e. we want to create a baseline for how the surface of this crystal looks after heating, in order to have something to compare it with when graphene eventually is grown on it.

First the STM must be calibrated. Since no known values can be measured on the Fe-22Cr surface, a highly oriented pyrolytic graphite (HOPG) was used. This was scanned on in the middle of this part of the project, which concerned the Fe-22Cr investigations. Using images from HOPG a calibration was done. The parameter was found to be

$$X : 0.955, Y : 1.054 \quad (4.2)$$

Here there is also an off-set caused by drift in the STM.

In figure 4.4 the clean surface of the Fe-22Cr crystal is shown. It was cleaned by sputter and anneal, described in section 3.4. This was done at a sputter pressure of $4.4 \times 10^{-7} \text{ mbar}$ for 7 minutes, then a annealing to 900°C with a 7 minute holding

RESULTS

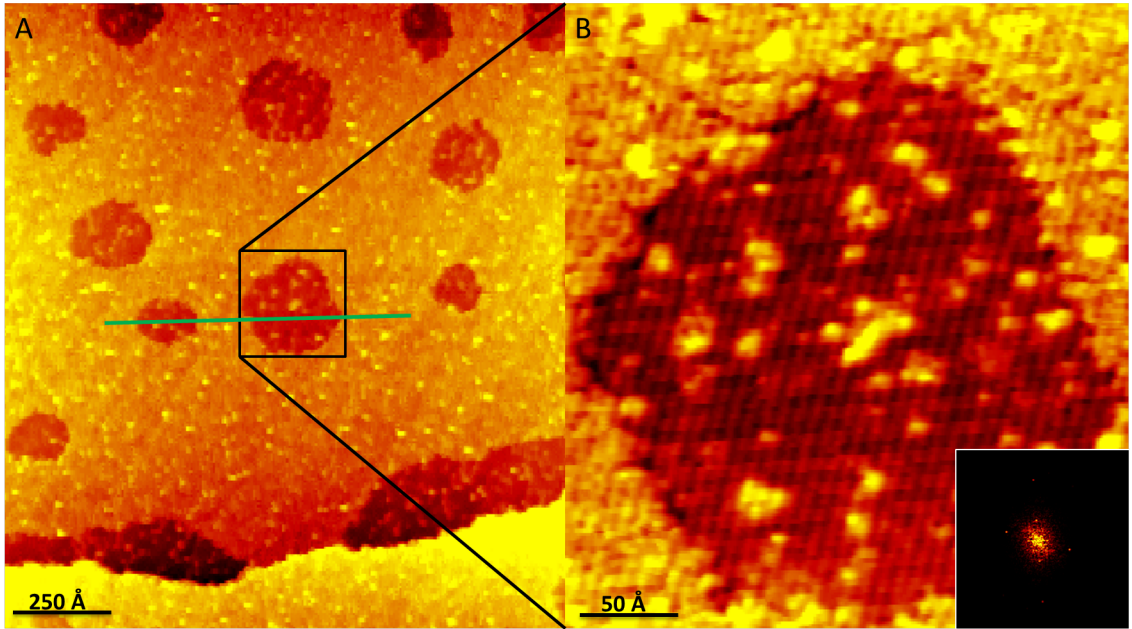


FIGURE 4.5: Two STM images of the clean Fe-22Cr surface after heating to 600°C for 15 minutes. (B) is the zoom indicated in (A). The insert on (B) shows the FFT of that image. Using this FFT it is found that the structure which is visible on (B) is noise, since the structure can be removed by filtering away two pixel-sized dots on the FFT. The green line on (A) represents the line scan in figure 4.6B. (A) $I = 0.310 \text{ nA}$, $V = 1317.1 \text{ mV}$, (B) $I = 0.350 \text{ nA}$, $V = 1238.7 \text{ mV}$.

at maximum temperature, which was repeated 29 times. Even though the FFT of the image has been filtered, it is still blurry and noisy. This is properly due to a bad and unstable tip or an unstable surface.

The crystal was then heated to 600°C for 15 minutes, with a temperature ramp of 1 K/s both up and down. Two images of the crystal after heating are shown in figure 4.5. The surface has clearly changed during the heating process. Dark dots are now observed on the surface. Also light spots which are smaller in size are visible all over the surface. In both figure 4.4 and 4.5A a step edge is visible. These step edges have been measured to have a height of $1.2 \pm 0.2 \text{ Å}$. This is, however, without any calibration of the STM in the z-direction. The big spots on figure 4.5 are of the same depth as the unevenness on the surface before heating in figure 4.4. To clarify this a line scan of each of the two surfaces is shown in figure 4.6. Here it is seen that after heating the holes on the sample are much more distinct than the roughness of the sample before heating, i.e. the surface looks more smooth, but with clear indications of holes after annealing.

To clarify this Auger electron spectroscopy (AES) was performed on the crystal before and after heating. These Auger spectra are compared in figure 4.7.

RESULTS



FIGURE 4.6: Comparison of the line scans from figure (A): 4.4 and (B): 4.5A. (B) Shows that the holes have a much more distinct depth, where as the surface from (A) is more rough.

Measured energy [eV]	Reference energy [eV]	Corresponding element
277	275	Carbon*
451	450	Chromium
463	461	Chromium
484	484	Chromium
496/500	491	Chromium
518/521	519	Iron
535	513	Chromium*
581	571	Chromium
606	600	Iron
661	654	Iron
714/716	705	Iron*

TABLE 4.1: Table showing the measured energies, from figure 4.7, the reference energies and the corresponding element. The reference energies is from reference spectra [26]. *Distinct peak.

RESULTS

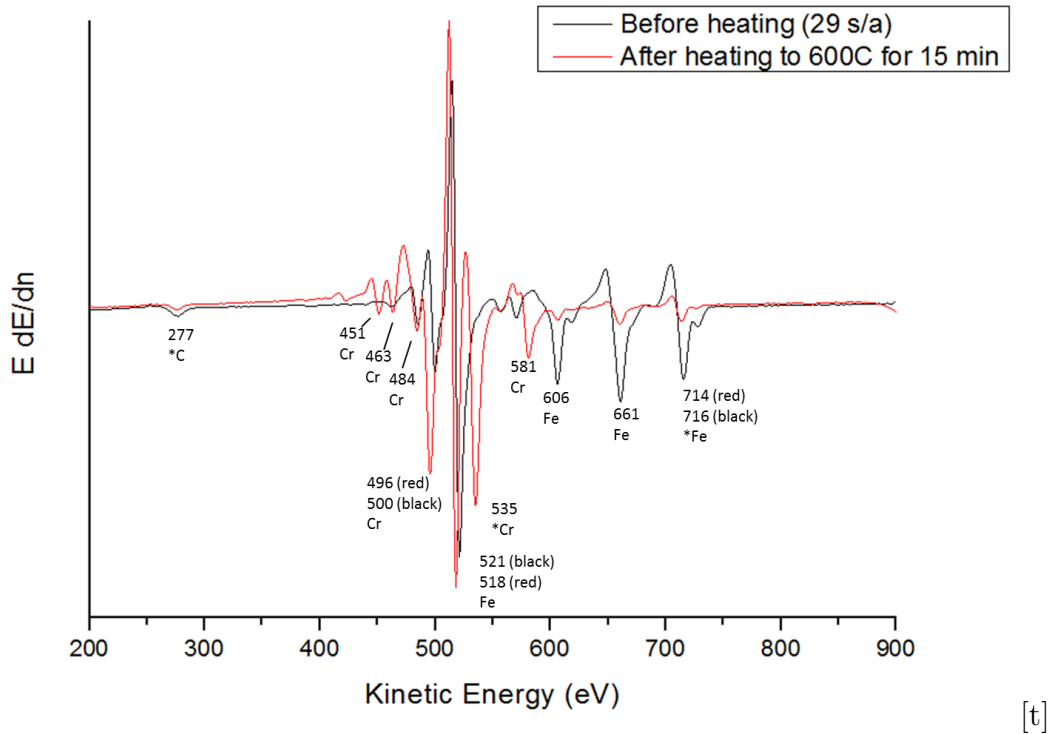


FIGURE 4.7: Comparison of the two Auger spectra, before and after heating. For reference of the energies see table 4.1. *Distinct peak.

Before analysing the AES data one should note that it appears that the spectra have some sort of off-set, meaning that the peak in the spectra did not lie at the same energy level as the reference spectra. In order to get a value for this off-set it was tried to scan on a sample on which we were sure where the peaks should be. For this HOPG was tried. Unfortunately the off-set on HOPG was no where near the off-set of other scanned crystals, such as the Fe-22Cr. Therefore we cannot put a general value on the off-set, but have to consider a new value for every scan. Further analysis also showed that the off-set is not linear throughout the scan. These off-set problems does, however, not cause big problems, since it is still possible make a reasonable guess on which elements gives certain peaks in the spectra. Therefore no calibration on the AES data was done. It is also possible that this off-set is not a off-set at all, but could perhaps be created by chemical shifts. The AES method does, however, measure the energy difference in the atoms orbital shell, which should be very distinct and not affected by chemical shifts.

When looking at the spectra comparison in figure 4.7, it is clear that there is a change. This change seems to be that the peaks for chromium are higher while the peaks for the iron are lower after heating. These changes indicate a higher concentration of chromium and a lower concentration of iron in the surface. In

RESULTS

order to see which energies corresponds to which element in the reference spectra see table 4.1.

Combining the AES data, which shows more chromium at the surface, and the STM data showing some holes, this could indicate a top layer of chromium has covered the surface. The holes would then be places where the chromium is not covering the Fe-22Cr surface.

This result correspond perfectly to what other project has pointed to; when heating a Fe-Cr alloy chromium migrates to the surface seen as an increase in the intensity of the chromium peak in the Auger spectrum [19, 20, 21].

The result described in this section is only from one measurement. To fully give an answer to what happens with the surface, when the crystal is heated, more measurements are needed. These further measurements should be obtained after different temperature heatings and different holding times. Furthermore scanning tunnelling spectroscopy (STS), which measured the electron density, could be used. This could then be used to identify the specific element at the hole sites. With this it could be confirmed if it really is the Fe-22Cr crystal that is seen there. We did not achieve further measurements due to several problems which needed to be solved. The list of problems includes leaks in several valves, filaments shorting and breaking, thermocouple wires melting, AES control computer shorted, noise problems in the STM properly due to a grounding problem. To fix most of the problems the chamber had to be opened, fixed, closed and then baked. Depending on the problem this procedure took two or more days to complete. The noise problem was never really fixed, but could perhaps be caused by a major renovation taking place during lab time at the Physics and Astronomy Department at Aarhus University.

5 Conclusion

The first part of this project, where graphene was grown on iridium, was very successful. We were able to grow good quality graphene with only minor defects and impurities. Chemical vapour deposition (CVD) proved to be an effective method to grow the graphene. This method was reasonably quick. The graphene was also of high quality and spaced over large terraces on the iridium surface.

The second part of the project, investigations of the surface of the Fe-22Cr crystal, proved to be more difficult. The focus was aimed at investigating what happens to the surface when it is heated, simulating a recipe that might be used for graphene growth. Our results showed that the chromium migrates towards the surface during heating. This can be seen as increases in the intensity peaks for the chromium elements in Auger electron spectroscopy (AES) data. Furthermore the chromium migration was observed to change the surface topography on the scanning tunnelling microscope (STM) images. The results correspond to results published by others, as mentioned in section 2.3. Although the quality of the STM data exceeds that available in the references.

5.1 Outlook

Further work on graphene on iridium has already been done in the group. The graphene can be functionalized, meaning that molecules are dosed on to change the properties of graphene. This was done by Daniel Tejero Martin, former bachelor student at the SDL group, together with Andrew Cassidy. To make the graphene usable in e.g. electronic applications, it should be transferred from the iridium to a semiconductor or insulator, SiO_2 as an example. This is rather difficult due to the previous mentioned interactions between the carbon and iridium atoms. All the graphene on iridium samples grown in this project were passed on to a group of chemists at Aarhus University, who were trying to do this transfer. They have had success with transferring graphene from copper, but here the interactions are weaker, which also gives out graphene with a lot of different orientations, meaning worse

CONCLUSION

quality. Their project to transfer graphene from iridium has had some promising initial result, but more studies are needed.

This short project provided some insight in the changes of the Fe-22Cr surface in responds to heating. In order to begin graphene growth on the crystal a more in-depth study is required. suggestions for beginning this study includes checking the reproducibility of the results presented here. Furthermore scanning tunnelling spectroscopy (STS) data could be acquired. It would also be very interesting to introduce the clean Fe-22Cr crystal to an oxygen rich atmosphere, in order to investigate what happens when the crystal is oxidized. Finally the surface should be exposed to ethylene in order to try growing graphene. This project has showed that STM combined with AES is a good strategy for approaching these experiments.

Bibliography

- [1] A. K. Geim. Graphene: status and prospects. *Science*, 324(5934):1530–4, 2009.
- [2] A. K. Geim and K. S. Novoselov. The rise of graphene. *Nature materials*, 6(3):183–191, 2007.
- [3] R. Balog, B. Jørgensen, L. Nilsson, M. Andersen, E. Rienks, M. Bianchi, M. Fanetti, E. Lægsgaard, A. Baraldi, S. Lizzit, Z. Sljivancanin, F. Besenbacher, B. Hammer, T. G. Pedersen, P. Hofmann, and L. Hornekær. Bandgap opening in graphene induced by patterned hydrogen adsorption. *Nature materials*, 9(4):315–9, 2010.
- [4] K. S. Novoselov, V. I. Fal’ko, L. Colombo, P. R. Gellert, M. G. Schwab, and K. Kim. A roadmap for graphene. *Nature*, 490(7419):192–200, 2012.
- [5] H. D. Young and R. A. Freedman. *University Physics*. Pearson Education Inc., 13th edition, 2010.
- [6] K. S. Novoselov, A. K. Geim, S. V. Morozov, D. Jiang, Y. Zhang, S. V. Dubonos, I. V. Grigorieva, and A. A. Firsov. Electric field effect in atomically thin carbon films. *Science*, 306(5696):666–669, 2004.
- [7] L. Gao, J. R. Guest, and N. P. Guisinger. Epitaxial graphene on Cu(111). *Nano letters*, 10(9):3512–6, 2010.
- [8] S. Bae, H. Kim, Y. Lee, X. Xu, J.-S. Park, Y. Zheng, J. Balakrishnan, T. Lei, H. R. Kim, Y. I. Song, Y.-J. Kim, K. S. Kim, B. Ozyilmaz, J.-H. Ahn, B. H. Hong, and S. Iijima. Roll-to-roll production of 30-inch graphene films for transparent electrodes. *Nature nanotechnology*, 5(8):574–8, 2010.
- [9] L. Nilsson, M. Andersen, R. Balog, E. Lægsgaard, P. Hofmann, F. Besenbacher, B. Hammer, I. Stensgaard, and L. Hornekær. Graphene coatings: probing the limits of the one atom thick protection layer. *ACS nano*, 6(11):10258–66, 2012.

BIBLIOGRAPHY

- [10] S. Chen, L. Brown, M. Levendorf, W. Cai, S.-Y. Ju, J. Edgeworth, X. Li, C.W. Magnuson, A. Velamakanni, R.D. Piner, J. Kang, J. Park, and R.S. Ruoff. Oxidation resistance of graphene-coated Cu and Cu/Ni alloy. *ACS nano*, 5(2):1321–7, 2011.
- [11] D. Prasai, J.C. Tuberquia, R.R. Harl, G.K. Jennings, B.R. Rogers, and K.I. Bolotin. Graphene: corrosion-inhibiting coating. *ACS nano*, 6(2):1102–8, 2012.
- [12] R.K. Singh Raman, P. Chakraborty Banerjee, D.E. Lobo, H. Gullapalli, M. Sumandasa, A. Kumar, L. Choudhary, R. Tkacz, P.M. Ajayan, and M. Majumder. Protecting copper from electrochemical degradation by graphene coating. *Carbon*, 50(11):4040–4045, 2012.
- [13] J.S. Bunch, S.S. Verbridge, J.S. Alden, A.M. van der Zande, J.M. Parpia, H.G. Craighead, and P.L. McEuen. Impermeable atomic membranes from graphene sheets. *Nano letters*, 8(8):2458–62, 2008.
- [14] L. Nilsson, M. Andersen, B. Hammer, I. Stensgaard, and L. Hornekær. Breakdown of the Graphene Coating Effect under Sequential Exposure to O₂ and H₂S. *The Journal of Physical Chemistry Letters*, 4(21):3770–3774, 2013.
- [15] A. T. N'Diaye, J. Coraux, T. N. Plasa, C. Busse, and T. Michely. Structure of epitaxial graphene on Ir(111). *New Journal of Physics*, 10(4):043033, 2008.
- [16] P. Hofmann. http://philiphofmann.net/ultrahighvacuum/basic_physics.html, Basic physics behind UHV, December 2013.
- [17] D. A. Porter, K. E. Easterling, and M. Y. Sherif. *Phase Transformations in Metal and Alloys*. Taylor & Francis Group, 3rd edition, 2009.
- [18] J.-O. Andersson and B. Sundman. Thermodynamic properties of the CrFe system. *Calphad*, 11(1):83–92, 1987.
- [19] J. S. Lin, H. Cabibil, B. Ekstrom, and J. A. Kelber. STM, LEED and AES studies on the oxidation of a CrN overlayer on Fe0.8Cr0.2(100). *Surface Science*, 371(2-3):337–348, 1997.
- [20] H. Ali-Löytty, P. Jussila, M. Hirsimäki, and M. Valden. Influence of CrN surface compound on the initial stages of high temperature oxidation of ferritic stainless steel. *Applied Surface Science*, 257(17):7783–7791, 2011.

BIBLIOGRAPHY

- [21] M. Legrand, B. Diawara, J.-J. Legendre, and P. Marcus. Three-dimensional modelling of selective dissolution and passivation of ironchromium alloys. *Corrosion Science*, 44(4):773–790, 2002.
- [22] J. Tersoff and D. R. Hamann. theory and application of scanning tunnelling microscopy. *Physical Review Letters*, 50(25):1998–2001, 1983.
- [23] J. Tersoff and D. R. Hamann. Theory of the scanning tunneling microscope. *Physical Review B*, 31(2):805–813, 1985.
- [24] J. Bardeen. Tunnelling from a Many-Particle Point of View. *Physical Review Letters*, 6(2):57–59, 1961.
- [25] P. Hofmann. *Lecture Notes on Surface Science; Aarhus University course*. 2005.
- [26] K. D. Childs, B. A. Carlson, L. A. LaVanier, J. F. Moulder, D. F. Paul, W. F. Stickle, and D. G. Watson. *Handbook of Auger Electron Spectroscopy*. Physical Electronics, Inc., Eden Prairie, Minnesota, 3rd edition, 1995.
- [27] M.F. Chung and L.H. Jenkins. Auger electron energies of the outer shell electrons. *Surface Science*, 22(2):479–485, 1970.
- [28] P. Hofmann. http://philiphofmann.net/ultrahighvacuum/ind_rotaryvane.html, Rotary vane pumps, January 2014.
- [29] P. Hofmann. http://philiphofmann.net/ultrahighvacuum/ind_roughing.html, Roughing pump, January 2014.
- [30] P. Hofmann. http://philiphofmann.net/ultrahighvacuum/ind_turbopump.html, Turbo pump, January 2014.
- [31] P. Hofmann. http://philiphofmann.net/ultrahighvacuum/ind_ionpump.html, Ion pump, January 2014.
- [32] P. Hofmann. http://philiphofmann.net/ultrahighvacuum/achieving_UHV.html, Achieving UHV, January 2014.
- [33] P. Hofmann. http://philiphofmann.net/ultrahighvacuum/ind_bakeout.html, Bakeout, January 2014.
- [34] G. Binnig, H. Rohrer, Ch. Gerber, and E. Weibel. Surface Studies by Scanning Tunneling Microscopy. *Physical Review Letters*, 49(1):57–61, 1982.

BIBLIOGRAPHY

- [35] http://specs.de/cms/upload/PDFs/SPECS_Prospekte/Aarhus_SPM_Family-Prospekt_2.pdf, Specs Aarhus SPM datasheet, January 2014.
- [36] <http://inano.au.dk/research/research-platforms/nanoanalysis/scanning-tunneling-microscopy>, Scanning tunneling microscopy, Nanoanalysis, January 2014.
- [37] <http://corning.com/WorkArea/showcontent.aspx?id=40321>, Macor datasheet, January 2014.
- [38] P. Hofmann. *Surface Physics: An Introduction*. Wiley-VCH Berlin, 2013.

A AES manual for the equipment on the Green Chamber

Here follows the complete detailed manual for use of the AES equipment on the Green Chamber.

1. When the sample is in the manipulator use these settings:
 - X: 20
 - Y: 7
 - Z: 23
 - θ : 137.5
2. When the sample is turned towards the Auger spectrometer, move the spectrometer towards the sample without the two touching ($\approx 1\text{mm}$ gap between them).
3. Turn on AES:
 - 3 main switches: Perkin-Elmer Electron Multiplier supply, Perkin-Elmer Digital AES control and the Electron Gun control.
 - On the Perkin-Elmer Electron Multiplier supply also switch CMA to digital.
 - On the Electron Gun control press the green button, which turns on the deflection of the electron beam, and afterwards the red button, which turns on the actual beam of electrons. The dials on the gauges will go up showing the voltage and current of the beam.

See figure A.1

4. Change computer (to STM97) by double tapping "scroll lock" on the keyboard.
5. Open the program "*Auger Acquisition*" from the desktop.



FIGURE A.1: A picture of the three control boxes for the AES equipment on the Green chamber.

6. The program is only controlled by the keyboard: Press "Esc", "Esc".
7. The control board cannot be found automatically, so the address is typed in manually in the settings: Press "Esc", pick option "*Change Settings*", pick "*interface Address*", type in "784", "Enter" - It should now read "*address is correct*". "Esc", "Esc" to exit settings menu
8. Select "*AES Spectrum*" this is where the AES is controlled.
9. Pick option 1 "*spectrum Parameters*" and set the settings required for the acquisition (Press "Enter" after changing each setting, exit with "Esc"):
 - "*Sweep Start*" (e.g. 200 eV)
 - "*Sweep End*" (e.g. 1100 eV)
 - "*Number of sweeps*" (e.g. 20; the spectrum acquired is an average of these)
10. Pick option 2 "*Extern parameters*" and set the setting required for the acquisition (Press "Enter" after changing each setting, exit with "Esc"):
 - "*SEV Volt (V)*" : 1100 (This is the voltage for the detector. This value is suitable most of the time. If the signal is just a straight line, turn the value up or down depending on whether the signal is too close to the bottom or the top of the screen.)

11. Everything is now ready. Pick "*Aquire survey*" to acquire a spectrum.
12. When the chosen number of spectra are completed it should be saved. Press "Esc" to exit the data display.
13. Select "*save ascii*".
14. Enter the address of an existing folder and type a name of maximum 8 characters, e.g. YYMMDDNO.txt (note .txt as ending)
15. Repeat 9-14 if more spectra are required and if another energy interval is wanted.
16. Now to close the program: "Esc", "Esc", it reads "*really quit*", press "Enter".
17. The program cannot close on its own, it must be forced. Press "Alt" + "TAB" to change back to the Windows desktop, right click on the program on the process bar and press "*close*", and then "*End now*".
18. Now the data should be moved in order to make it accessible for analysis on the analysis computer. On the desktop there are two short cuts to two different folders, open both of them. Copy/Paste the newly acquired data from the local folder to the shared folder.
19. Now change back to the first computer by double tapping "scroll lock" on the keyboard. Analyse the data using Origin 8 or similar.

The data can be compared with reference spectra [26].